Pulse-timing symmetry breaking in an excitable optical system with delay

Soizic Terrien,[1,*] Venkata A. Pammi,[2] Bernd Krauskopf,[1] Neil G. R. Broderick,[1] and Sylvain Barbay[2]
[1]*The Dodd-Walls Centre for Photonic and Quantum Technologies, The University of Auckland, New Zealand*
[2]*Université Paris-Saclay, Centre National de la Recherche Scientifique, Centre de Nanosciences et de Nanotechnologies, Palaiseau, France*

(Received 11 June 2020; accepted 10 November 2020; published 13 January 2021)

Excitable systems with delayed feedback are important in areas from biology to neuroscience and optics. They sustain multistable pulsing regimes with different numbers of equidistant pulses in the feedback loop. Experimentally and theoretically, we report on the pulse-timing symmetry breaking of these regimes in an optical system. A bifurcation analysis unveils that this originates in a resonance phenomenon and that symmetry-broken states are stable in large regions of the parameter space. These results have impact in photonics for, e.g., optical computing and versatile sources of optical pulses.

DOI: 10.1103/PhysRevE.103.012210

I. INTRODUCTION

Time periodic regular pulsing regimes can emerge in many dissipative physical systems with delayed feedback [1,2]. This phenomenon is encountered in various fields, from neurosciences [3,4] to optics and opto-electronics [5–8], ecology [9], and chemistry [10,11]. Typically, these systems are multistable, with several coexisting regular periodic regimes [12,13]. Multistability has been shown to be of particular interest for all-optical processing capabilities, e.g., associative memories [14–16].

Here we consider an excitable optical system with delayed feedback, namely, a micropillar laser with integrated saturable absorber and delayed optical feedback. In the excitable regime and for a sufficiently large delay time, the system regenerates its own output at regular time intervals [17–20]: if a short duration perturbation with sufficiently large amplitude is sent as an input, the system emits a light pulse which is re-injected by the feedback loop after a delay time τ. If the losses in the feedback loop are sufficiently low, the re-injected pulse is regenerated in the excitable medium. As the process repeats, this results in a periodic pulsing regime with period T slightly larger than τ due to the finite response time of the excitable medium.

When several perturbations are sent sequentially, the timing structure of the regenerated pulses in the feedback loop persists in the short term. This can lead to interesting applications such as optical buffer memories [17–20]. However, in optics, most of the excitable or pulsing systems with delayed feedback [16–18,21] show a convergence in the long term to self-pulsing regimes consisting of *equidistant* pulses in the feedback loop. In a vertical cavity surface emitting laser (VCSEL) system subject to long opto-electronic feedback, the repulsion of two pulses has been reported, leading to a nonequidistant pulsing regime [22].

We report here on a pulse-timing symmetry-breaking phenomenon, where some symmetric regimes destabilize and the long-term stable dynamics consists of coexisting equidistant and nonequidistant pulses in the feedback loop. This is observed experimentally and analyzed in a mathematical model, which takes the form of a system of three coupled delay-differential equations (DDEs). A bifurcation analysis unveils that the observed nonequidistant pulsing dynamics results from destabilising bifurcations of the equidistant pulsing solutions; these occur when the delay τ is increased, provided that the recombination rate of carriers in the gain medium is faster than the one of the saturable absorber. We show that the emergence of stable pulsing patterns with n nonequidistant pulses is generic in the system and arises from symmetry breaking due to locked dynamics on invariant tori. Two stable nonequidistant pulses in the feedback loop emerge from a period-doubling bifurcation of the equidistant two-pulse solution, which is close to a $1:2$ strong resonance. Because of the amplitude-timing coupling in the excitable system [23,24], the relative timings of the pulses are very strongly affected. This is responsible for the observed immediate symmetry breaking of pulse timings. Pulsing patterns with n equidistant pulses per feedback loop with $n \geqslant 3$ destabilize in torus bifurcations that are close to $1:n$ resonance. This results in large resonance tongues, i.e., regions of the parameter space where the dynamics on the torus is locked. Due to the amplitude-timing coupling, these locked $1:n$ periodic orbits correspond here to higher-order symmetry-broken, nonequidistant pulsing regimes. We show that nonequidistant and equidistant pulsing regimes can coexist, thus leading to a much increased level of multistability of pulsing patterns.

II. MODEL EQUATIONS

We consider the Yamada equations with incoherent delayed feedback [25,26], a model of a semiconductor laser written in the form of three DDEs for the dimensionless gain G, absorption Q, and intracavity intensity I:

$$\dot{G} = \gamma_G(A - G - GI); \quad \dot{Q} = \gamma_Q(B - Q - sQI);$$
$$\dot{I} = (G - Q - 1)I + \kappa I(t - \tau). \tag{1}$$

*s.terrien@auckland.ac.nz

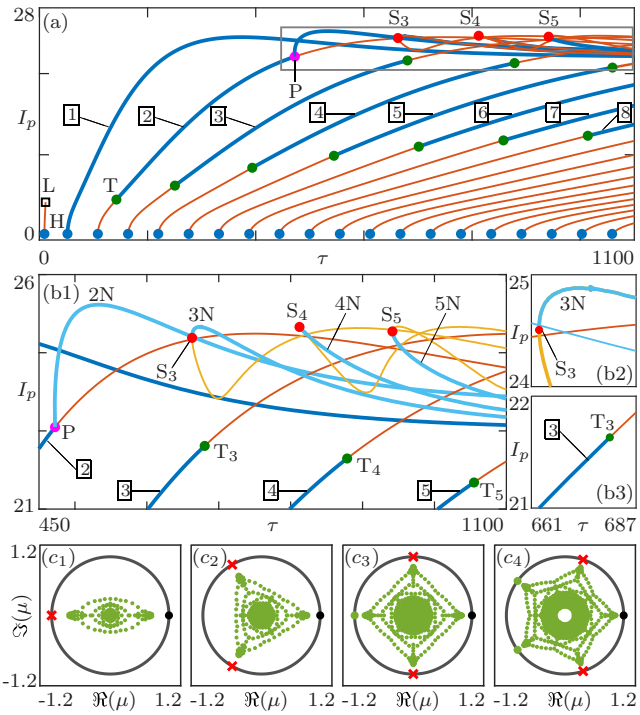

FIG. 1. (a) Bifurcation diagram of (1), showing the pulse intensity I_p with respect to τ, with the number of pulses per feedback loop along each stable periodic solution branch. (b1) Enlargement of the framed area in (a), with further enlargments around point (b2) T_3 and (b3) S_3. Stable equidistant (E) and nonequidistant (N) pulse solutions are represented in dark and light blue, respectively, and unstable E and N solutions in dark and light orange, respectively. The dots indicate Hopf (H), torus (T), period doubling (P), saddle-node (S), and homoclinic (L) bifurcations. (c1)–(c4) Floquet multipliers at points P, T_3, T_4, and T_5, with critical multipliers highlighted in red.

The time variables are rescaled with respect to the cavity photon lifetime [27]. Here, A is the pump parameter, B is the nonsaturable absorption, s is the scaled saturation parameter, γ_G and γ_Q are the recombination rates of the carriers in the gain and absorber media, respectively, and κ and τ are the feedback strength and delay, respectively. Unless stated otherwise, we consider the following parameter values: $A = 2$, $B = 2$, $\gamma_G = 0.01$, $\gamma_Q = 0.055$, $s = 10$, and $\kappa = 0.2$. The delay time τ is considered as a bifurcation parameter. This model has been shown to produce rich and complex dynamics [26,28], and to describe accurately the dynamics of an excitable micropillar laser with integrated saturable absorber subject to delayed optical feedback [16,20]. We study the DDE (1) here in a parameter regime that has not been considered before, namely, in the situation when γ_G is smaller than γ_Q so that the carriers of the gain G recombine faster than those of the absorbtion Q.

III. BIFURCATION ANALYSIS

Figure 1(a) shows the one-parameter bifurcation diagram of system (1) in the delay time τ, where solutions are represented by their maximum value I_p of intensity I. When τ increases from zero, successive Hopf bifurcations (H) are encountered, from which several branches of coexisting periodic solutions emerge. Far from the Hopf bifurcations, these solutions correspond to the periodic emission of short light pulses, with periods close to submultiples of the delay [28] and with a fixed number of equidistant pulses in the feedback loop, as indicated in Fig. 1(a). The fundamental solution with one pulse per feedback loop appears at $\tau = 51.7$ and is stable for any larger value of τ. On the other hand, all the n-pulses solutions with $n \geqslant 2$ emerge unstably from a Hopf bifurcation, subsequently stabilize in a torus bifurcation (T) when τ increases and finally destabilize through a second bifurcation. All these solutions coexist with the zero-intensity equilibrium solution (i.e., the nonlasing solution), which is stable over the entire range of τ in Fig. 1(a).

Figure 1(b) presents the enlargements of Fig. 1(a) near the destabilizing bifurcations of the equidistant pulsing regimes with two to five pulses (points P, T_3, T_4, and T_5, respectively), and Fig. 1(c) show the Floquet multipliers at these points. The two-pulse solution destabilizes at point P through a period-doubling bifurcation, with one Floquet multiplier crossing the unit circle at -1 [Fig. 1(c1)]. This bifurcation is close to a $1:2$ resonance point, where two Floquet multipliers are equal to -1 [29]. The three-, four-, and five-pulse solutions destabilize at torus bifurcations T_3, T_4, and T_5, respectively, where two complex conjugate Floquet multipliers cross the unit circle. These critical Floquet multipliers are extremely close to $e^{\pm i2\pi/n}$, showing that the torus bifurcations are close to $1:n$ resonance points with $n = 3$, 4, and 5, respectively [see Figs. 1(c2) to 1(c4)]. As a consequence, instead of the quasiperiodic regime one would expect after the bifurcation, one observes locked periodic solutions winding n times around the torus. These emerge at the saddle-node bifurcations S_n. As will be discussed below, the new locked pulsing regimes correspond to nonequisitant pulsing patterns. From a physical point of view, this means that critical values of the delay exist for which the equidistant periodic solutions lose stability in favor of nonequidistant pulsing regimes.

The destabilization of the two-pulse periodic regime at point P leads to a period-doubled regime with two nonequidistant pulses per feedback loop and thus appears as a pulse-timing symmetry broken state. This is illustrated in Fig. 2(a), which shows the evolution of the amplitudes and relative timings of pulses with respect to τ, along the branches of solutions corresponding to two equidistant and two nonequidistant pulses. After the period doubling bifurcation at $\tau = 472$, one observes both a splitting of the pulse amplitudes in Fig. 2(a1) (as expected), but also a strong splitting or symmetry breaking of the relative pulse timings [Fig. 2(a2)], which is due to the strong time-amplitude coupling of the system [16,30].

We use numerical simulations to further assess how the regime with two nonequidistant pulses is accessed. Figure 2(b) shows, for $\tau = 1000$, the long-term dynamics of system (1) when it is initially on the (unstable) equidistant two-pulse solution and subsequently slightly perturbed by increasing the gain variable G. The system slowly converges to one of the two possible nonequidistant stable pulsing patterns: the first pulse timing interval decreases [Fig. 2(b2)] and the second pulse (highlighted in gray) converges towards a low amplitude state [Fig. 2(b1)]. When a different initial

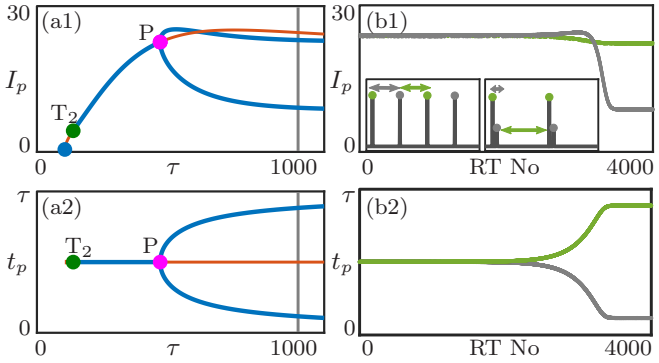

FIG. 2. (a1) Maximum I_p of pulse intensity and (a2) relative interpule timings t_p along the branches of two equidistant and two nonequidistant pulses, with respect to τ. Stable and unstable solutions are represented in blue and red, respectively. (b) Simulation of (1) for $\tau = 1000$ [gray lines in panel (a)] with initial condition very near the (unstable) two-pulse solution, showing the long-term evolution of (b1) I_p and of (b2) t_p. The subpanels in (b1) show the intensity time series during the two first and two last roundtrips through the feedback loop; the dots and arrows indicate the amplitudes and relative timings as represented in (b1) and (b2), respectively.

perturbation is applied by depleting G slightly (not shown here), the phase-shifted, symmetric version of this solution is obtained, with the first (green) and second (gray) pulses converging to the low-amplitude and high-amplitude states, respectively. Although this leads seemingly to the same long-term dynamics, both of these different states occur, one being a phase-shifted version of the other. We also point out that the convergence is very slow and occurs over several thousand of delay times, showing that the stable nonequidistant solutions are only weakly attracting.

The bifurcation mechanism leading to the emergence of nonequidistant pulsing regimes with more than three pulses is slightly different. As shown in Fig. 1(b1), a pair of (stable or unstable) periodic solutions emerges from a saddle-node bifurcation, for example, at $\tau = 663$ for $n = 3$. This bifurcation forms the boundary of the $1:n$ resonance tongue associated with the destabilizing torus bifurcation of the n-pulse solution. The emerging periodic solutions have a period close to τ, compared to the period close to τ/n of the n-pulse solution undergoing the torus bifurcation. Here the stable $1:n$ locked periodic solution corresponds to a pulsing regime with n nonequidistant pulses of different amplitude in the feedback loop. As such, the $1:n$ resonance tongues are identified here as the stability regions of nonequidistant pulsing solutions. Their emergence leads to a rapidly increasing level of multistability.

Figure 3(a) shows the intensity profiles of the coexisting stable periodic solutions for $\tau = 1000$. Here the nonequidistant two-, three-, four-, and five-pulse solutions [Figs. 3(a2) to 3(a5)] coexist with the stable one-pulse solution [Fig. 3(a1)], but also with the stable solutions with five, six, and seven equidistant pulses in the feedback loop [Figs. 3(a5) to 3(a7)]. Overall, when τ is increased, more and more of the equidistant pulsing regimes become unstable, while more and more stable periodic solutions with nonequidistant pulses in the feedback loop appear. Typically, for sufficiently large τ, solutions with lower numbers of (at least two) nonequidistant pulses coexist with solutions with larger numbers of equidistant pulses. In Fig. 3, all the periodic solutions with one to seven pulses per feedback loop coexist, but the ones with two to five pulses already underwent the resonance tongue transition and, thus, correspond to nonequidistant pulsing patterns.

Figure 3(b) presents the regions of stability in the (τ, κ)-plane of feedback parameters of the different pulsing regimes with one up to eight (equidistant and nonequidistant) pulses per feedback loop. Here the regions of stability of the nonequidistant pulsing solutions are resonance tongues bounded by saddle-node bifurcations. The respective stability regions of both types of solutions extend over large areas of the (τ, κ) parameter plane. Moreover, they show a large degree of overlap, which is why we show them in individual panels [Figs. 3(b1) to 3(b8)] for one up to eight pulses per feedback loop. This represents the high degree of multistability between all the different solutions represented in Fig. 3(a); indeed, the long-term convergence to one or the other pulsing solution depends on the chosen initial conditions. Interestingly, for $n \geqslant 3$ both the solutions with n equidistant pulses and with n non-equidistant pulses may coexist and be stable for the same parameter values. As shown in Fig. 1(b1), this results from the fact that the $1{:}n$ resonance tongues are entered (at points S_n) slightly before the n-pulse solutions destabilize

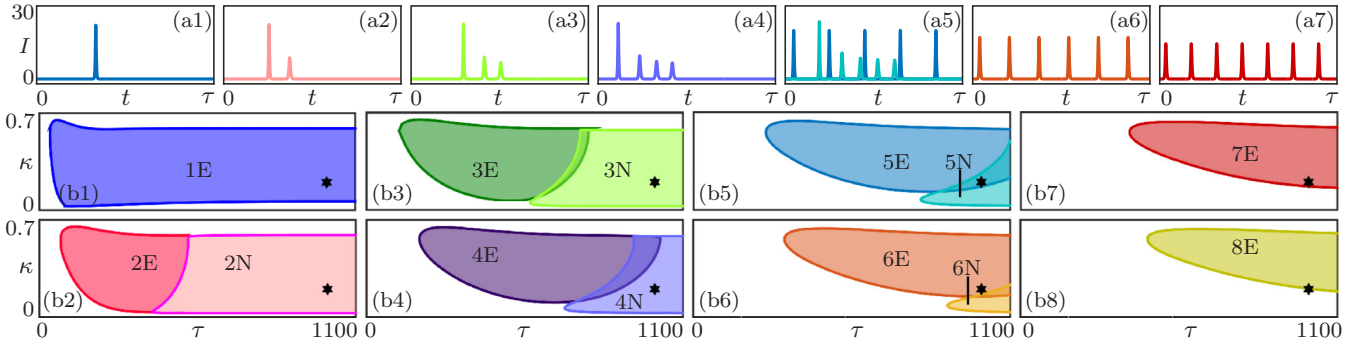

FIG. 3. (a) Intensity profiles of coexisting periodic solutions of (1), for $\tau = 1000$ and $\kappa = 0.2$. (b) Regions of stability, in the (τ, κ)-plane of feedback parameters, of the families of equidistant (E) and nonequidistant (N) periodic solutions with one to eight pulses per feedback loop. The number of pulses is indicated in the colored regions, and the star indicates the parameter point $(\tau, \kappa) = (1000, 0.2)$ of the time series in panels (a).

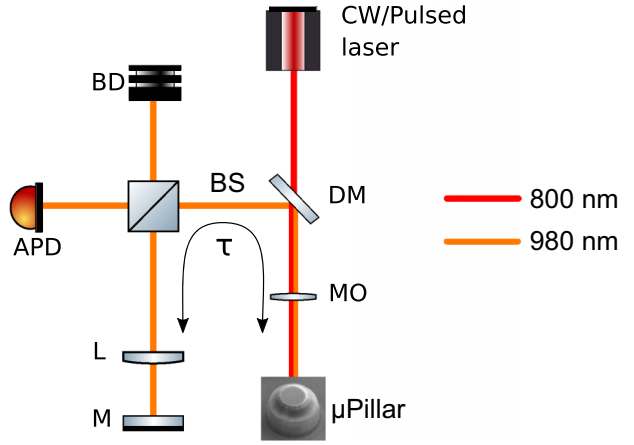

FIG. 4. Schematic of the experimental setup showing the optically pumped excitable micropillar laser with delayed optical feedback from an external mirror. DM: Dichroic mirror; BS: Beam splitter with 70/30 power split between reflected and transmitted path; MO: Microscope objective; APD: Avalanche photodiode; L: Lens with $f = 5$ cm, M: High reflectivity feedback mirror; BD: Beam dump; μPillar: Micropillar laser; τ: External cavity round trip time.

at torus bifurcation points T_n. Hence, in these ranges of τ, depending on the initial condition, one observes a pattern with n either equidistant or nonequidistant pulses. In particular, in Fig. 3(a5) both the solutions with five equidistant and five nonequidistant pulses coexist for the considered values of the parameters; see also Fig. 3(b5).

IV. EXPERIMENTAL REALIZATION

We compare the results of the bifurcation analysis with experimental measurements of an excitable micropillar laser. It consists of two gain and one saturable absorber (SA) quantum wells [31,32], is optically pumped with a cw laser at 800 nm and emits light at a wavelength around 980 nm. The micropillar has a vertical microcavity structure with two optimized multilayer semiconductor mirrors [31], a 2λ cavity thickness and a 5 μm diameter. It is coated with a 2 μm thick SiN layer for better heat management and protection from oxidation. The output light from the micropillar is split using a $R/T = 70/30$ beamsplitter (BS). The transmitted part is detected with a 5 GHz bandwidth avalanche photodiode (APD), amplified by a large bandwidth (18 GHz) RF amplifier and analyzed with a 13 GHz oscilloscope. The reflected part is directed into an external cavity, closed by a high-reflectivity mirror (M) after focusing with a 5 cm focal length lens, which provides a delay τ on the order of 10 ns, and is then reinjected into the micropillar laser. This delayed optical feedback results in a 10% reduction of the laser threshold. The experimental setup is sketched in Fig. 4 and it is similar to the one used in [20]. The micropillar laser is perturbed by short optical perturbations of 80 ps duration from a mode-locked Ti:Sa laser emitting around 800 nm. The micropillar laser with delayed optical feedback is pumped below the self-pulsing threshold. When the feedback strength is small, the system is in the excitable regime [33]: the steady state intensity I is zero, but

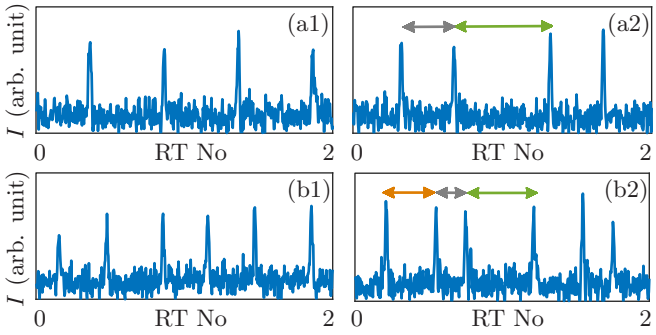

FIG. 5. Experimental intensity pulse trains shortly after (a1) two and (b1) three external perturbations, and after a large number of roundtrips in the external cavity with associated calibration of timings between the respective (a2) two and (b2) three sustained pulses; colored arrows indicate the interpulse timings as represented in Fig. 6. The feedback delay is 8.2 ns.

a single high-amplitude, short pulse of light can be emitted in response to an external perturbation of sufficient amplitude [27,34]. If the feedback strength is large enough, an excitable pulse is regenerated when it is reinjected by the delay loop after the delay τ, thus resulting in the regular emission of light pulses at a period close to τ [19,20].

In system (1) the ratio of the recombination rates γ_G and γ_Q of the gain and SA media, respectively, plays a crucial role in the pulsing dynamics [23,35,36]. In particular, the pulse-timing symmetry breaking is observed only for a faster gain recombination, that is, for $\gamma_G > \gamma_Q$. Experimentally, this unusual parameter regime can be accessed by selecting a suitable micropillar laser (from many on the same chip) by taking advantage of the spread of physical parameters in the course of the nanofabrication process.

Figure 5 shows intensity time traces generated by two and three external perturbations. We observe, shortly after they have been triggered by almost equally spaced perturbations, that the regenerated pulses are almost equidistant in the feedback cavity [Figs. 5(a1) and 5(b1)]. The pulses are sustained by the system effectively as long as the experiment is running, meaning that their number in the feedback cavity remains unchanged. In the long term, however, the timings between consecutive pulses calibrate to a nonequidistant pattern [Figs. 5(a2) and 5(b2)], showing clearly that the equidistant pulsing solution is not stable.

This is illustrated more clearly in Fig. 6, which shows the evolution of relative pulse timings of the experimental pulse trains (as indicated by the arrows in Fig. 5) over several hundreds of roundtrips in the feedback loop, in the same representation as in Fig. 2(b2). The experimental results in Fig. 6 are obtained for identical parameters but different initial conditions. In Figs. 6(a) and 6(b), the microlaser is started thanks to suitable external perturbations, close to the regimes with two and three equidistant pulses, respectively. We observe that the pulse-timing information is preserved in the short term [16,20]. On the other hand, in the long term, the system slowly converges towards nonequidistant pulsing patterns with well-defined and different interpulse relative timings. These interpulse timings then stay very stable over a large number of roundtrips. It was not possible to monitor

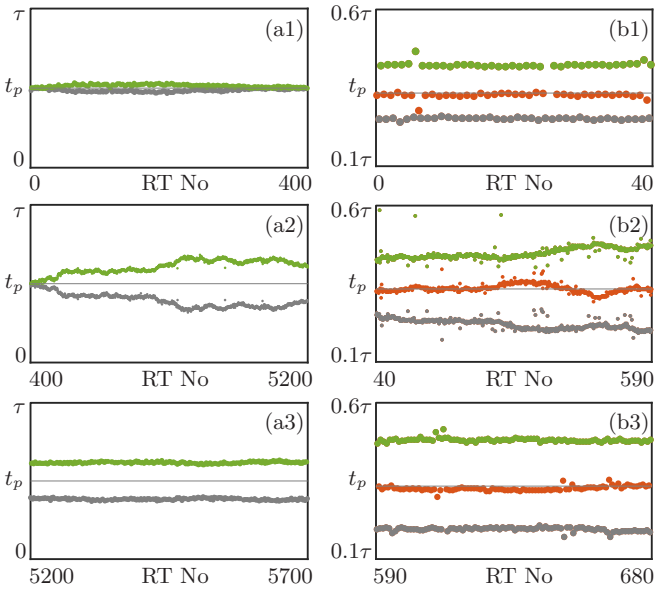

FIG. 6. Evolution over the roundtrip number of the relative interpulse timing t_p (as shown by arrows in Fig. 5) of experimental pulse trains following (a) two and (b) three external perturbations, for a feedback delay of $\tau = 8.2$ ns: just after the external perturbation [panels (1)], during the convergence towards nonequidistant pulsing patterns [panels (2)], and in the long-term [panels (3)].

the amplitude difference in the final state due to the limited signal to noise ratio — the emitted pulse energy is on the order of only 100 fJ. On the other hand, in agreement with Fig. 2, even a small difference in amplitude is associated with a large interpulse interval difference in the nonequidistant pulsing regime. Overall, the experimental observations show excellent agreement with the dynamics predicted by the bifurcation analysis of the model. They demonstrate multistability between the experimental regimes with two and three nonequidistant pulses. Moreover, the quasiperodic regime corresponding to unlocked dynamics on an invariant torus are not observed, in good agreement with the theoretical predictions of very large locking regions in the parameter space (see Fig. 3).

V. DISCUSSION AND CONCLUSION

We demonstrated that an optical excitable system with delayed feedback can sustain stable pulsing patterns with different numbers of nonequidistant pulses in the feedback loop. These arise from stable solutions with n equidistant pulses via torus bifurcations and associated $1:n$ resonances, which manifest themselves as a swift breaking of the timing-symmetry due to the strong amplitude-timing coupling of the excitable system. We find stable nonequidistant pulsing in large resonance tongues in the parameter space, bounded by saddle-node bifurcations of periodic solutions. As the delay is increased, there is a high and increasing degree of multistability between both symmetric and symmetry-broken pulsing patterns in the feedback loop. Which long-term behavior is observed depends on the initial condition. We demonstrated that nonequidistant pulsing can be observed reliably in an experiment with an excitable micropillar laser.

Our results are reminiscent of the pulsing dynamics of models in neuroscience that describe delay-coupled neurons either by a single limit cycle oscillator with delayed self-coupling [37,38] or by two limit cycle oscillators coupled through a time dependent synaptic response [39,40]. In our case, however, oscillations do not pre-exist and originate from the delayed feedback itself and their period is intimately linked to the delay time. This further illustrates that our results are expected to be generic and to extend beyond optics. Moreover, a mathematical connection between temporal dissipative solitons in spatially extended systems and pulsing regimes in delay systems has been recently suggested [30]. This raises open questions regarding possible connections between nonequidistant pulsing regimes and soliton molecules, which are bound states of pulses [41,42].

Beyond their fundamental interest for the nonlinear dynamics of delay systems, our results may contribute to the realization of nonconventional pulsing and reconfigurable optical sources [43], and to optical computing schemes [44–47] that rely on the large phase space available in delay systems [48].

ACKNOWLEDGMENTS

S.B. and V.A.P. acknowledge support from the CNRS Renatech Network of Technology for the nanofabrication of the samples.

[1] K. Pyragas, Phys. Lett. A **170**, 421 (1992).
[2] T. Erneux, *Applied Delay Differential Equations* (Springer, New York, 2009).
[3] A. Longtin and J. G. Milton, Math. Biosci. **90**, 183 (1988).
[4] S. A. Campbell, in *Understanding Complex Systems* (Springer, Berlin, 2007), pp. 65–90.
[5] K. Ikeda and O. Akimoto, Phys. Rev. Lett. **48**, 617 (1982).
[6] L. Illing and D. J. Gauthier, Physica D **210**, 180 (2005).
[7] Y. C. Kouomou, P. Colet, L. Larger, and N. Gastaud, Phys. Rev. Lett. **95**, 203903 (2005).
[8] M. C. Soriano, J. García-Ojalvo, C. R. Mirasso, and I. Fischer, Rev. Mod. Phys. **85**, 421 (2013).
[9] G. E. Hutchinson, Ann. N.Y. Acad. Sci. **50**, 221 (1948).
[10] I. R. Epstein and Y. Luo, J. Chem. Phys. **95**, 244 (1991).
[11] M. R. Roussel, J. Phys. Chem. **100**, 8323 (1996).
[12] J. Foss, A. Longtin, B. Mensour, and J. Milton, Phys. Rev. Lett. **76**, 708 (1996).
[13] J. Hizanidis, R. Aust, and E. Schöll, Int. J. Bifurcation Chaos **18**, 1759 (2008).
[14] P. R. Prucnal, B. J. Shastri, T. F. de Lima, M. A. Nahmias, and A. N. Tait, Adv. Opt. Photonics **8**, 228 (2016).
[15] M. A. Nahmias, B. J. Shastri, A. N. Tait, and P. R. Prucnal, IEEE J. Sel. Top. Quantum Electron. **19**, 1 (2013).

[16] S. Terrien, V. A. Pammi, N. G. R. Broderick, R. Braive, G. Beaudoin, I. Sagnes, B. Krauskopf, and S. Barbay, Phys. Rev. Research **2**, 023012 (2020).
[17] B. Garbin, J. Javaloyes, G. Tissoni, and S. Barland, Nat. Commun. **6**, 5915 (2015).
[18] B. Romeira, R. Avó, J. M. L. Figueiredo, S. Barland, and J. Javaloyes, Sci. Rep. **6** 19510 (2016).
[19] S. Terrien, B. Krauskopf, N. G. R. Broderick, L. Andréoli, F. Selmi, R. Braive, G. Beaudoin, I. Sagnes, and S. Barbay, Phys. Rev. A **96**, 043863 (2017).
[20] S. Terrien, B. Krauskopf, N. G. Broderick, R. Braive, G. Beaudoin, I. Sagnes, and S. Barbay, Opt. Lett. **43**, 3013 (2018).
[21] T. W. Carr, Phys. Rev. E **68**, 026212 (2003).
[22] F. Marino and G. Giacomelli, Chaos **27**, 114302 (2017).
[23] F. Selmi, R. Braive, G. Beaudoin, I. Sagnes, R. Kuszelewicz, T. Erneux, and S. Barbay, Phys. Rev. E **94**, 042219 (2016).
[24] T. Erneux and S. Barbay, Phys. Rev. E **97**, 062214 (2018).
[25] M. Yamada, IEEE J. Quantum Electron. **29**, 1330 (1993).
[26] B. Krauskopf and J. J. Walker, "Bifurcation study of a semiconductor laser with saturable absorber and delayed optical feedback," in *Nonlinear Laser Dynamics* (Wiley-VCH, Wenham, Germany, 2012), pp. 161–181.
[27] S. Barbay, R. Kuszelewicz, and A. M. Yacomotti, Opt. Lett. **36**, 4476 (2011).
[28] S. Terrien, B. Krauskopf, and N. G. R. Broderick, SIAM J. Appl. Dyn. Sys. **16**, 771 (2017).
[29] Y. A. Kuznetsov, *Elements of Applied Bifurcation Theory*, Vol. 112, (Springer Science & Business Media, New York, 2013).
[30] S. Yanchuk, S. Ruschel, J. Sieber, and M. Wolfrum, Phys. Rev. Lett. **123**, 053901 (2019).
[31] T. Elsass, K. Gauthron, G. Beaudoin, I. Sagnes, R. Kuszelewicz, and S. Barbay, Eur. Phys. J. D **59** 91 (2010).
[32] F. Selmi, R. Braive, G. Beaudoin, I. Sagnes, R. Kuszelewicz, and S. Barbay, Phys. Rev. Lett. **112**, 183902 (2014).
[33] J. L. A. Dubbeldam, B. Krauskopf, and D. Lenstra, Phys. Rev. E **60**, 6580 (1999).
[34] E. Izhikevich, Dynamical Systems in Neuroscience: The Geometry of Excitability and Bursting. (MIT Press, Cambridge, MA, 2007).
[35] J. L. A. Dubbeldam and B. Krauskopf, Opt. Commun. **159**, 325 (1999).
[36] R. Otupiri, B. Krauskopf, and N. G. Broderick, arXiv:1911.01835.
[37] V. Klinshov, L. Lücken, D. Shchapin, V. Nekorkin, and S. Yanchuk, Phys. Rev. Lett. **114**, 178103 (2015).
[38] V. Klinshov, L. Lücken, D. Shchapin, V. Nekorkin, and S. Yanchuk, Phys. Rev. E **92**, 042914 (2015).
[39] C. V. Vreeswijk, L. F. Abbott, and G. B. Ermentrout, J. Comput. Neurosci. **1**, 313 (1994).
[40] P. C. Bressloff and S. Coombes, SIAM J. Appl. Math. **60**, 820 (2000).
[41] P. Grelu and J. Soto-Crespo, *Lecture Notes in Physics* (Springer, Berlin, 2008), pp. 1–37.
[42] K. Krupa, K. Nithyanandan, U. Andral, P. Tchofo-Dinda, and P. Grelu, Phys. Rev. Lett. **118**, 243901 (2017).
[43] A. Aadhi, A. V. Kovalev, M. Kues, P. Roztocki, C. Reimer, Y. Zhang, T. Wang, B. E. Little, S. T. Chu, Z. Wang, D. J. Moss, E. A. Viktorov, and R. Morandotti, Opt. Express **27**, 25251 (2019).
[44] B. Romeira, J. M. L. Figueiredo, and J. Javaloyes, Chaos **27**, 114323 (2017).
[45] H. Peng, T. F. de Lima, M. A. Nahmias, A. N. Tait, B. J. Shastri, and P. R. Prucnal, in *2019 Conference on Lasers and Electro-Optics (CLEO)* (Optical Society of America, Washington, D.C., 2019), pp. 1–2.
[46] V. A. Pammi, K. Alfaro-Bittner, M. G. Clerc, and S. Barbay, IEEE J. Sel. Topics Quantum Electron. **26**, 1 (2020).
[47] J. Robertson, E. Wade, Y. Kopp, J. Bueno, and A. Hurtado, IEEE J. Sel. Topics Quantum Electron. **26**, 1 (2020).
[48] G. V. der Sande, D. Brunner, and M. C. Soriano, Nanophotonics **6**, 561 (2017).